DOI: 10.37190/abb/206980

Influence of anteromedial and central anterior cruciate ligament reconstruction on patellofemoral joint biomechanics during walking and running: a musculoskeletal modelling study

Yang Xiao[1], Chen Yang[2], Jie Xiang[3], Hongwei Li[4], Bin Chen[1*]

[1]Division of Orthopaedics and Traumatology, Department of Orthopaedics, Nanfang Hospital, Southern Medical University, Guangzhou, China

[2]College of Sports and Health, Shandong Sport University, Jinan, China

[3]Department of Orthopaedics and Traumatology, The First Affiliated Hospital, Hengyang Medical School, University of South China, Hengyang, China

[4]School of Mechanical Engineering, North University of China, Taiyuan, China

[*]Corresponding author: Bin Chen, Division of Orthopaedics and Traumatology, Department of Orthopaedics, Nanfang Hospital, Southern Medical University, Guangzhou, China, e-mail address: chb@smu.edu.cn

Submitted: 1st April 2025

Accepted: 11th June 2025

Abstract

Purpose: This study investigated the effect of anteromedial (AM) and central anterior cruciate ligament (ACL) reconstructions on the patellofemoral joint (PFJ) contact mechanics during walking and running.

Methods: Six knee models were established under a musculoskeletal multibody dynamic framework. The ACL attachment points and muscle volume of the quadriceps femoris and hamstrings were modified to simulate ACL reconstructions and post-operative muscle atrophy. Walking and running simulations were performed to quantify ACL graft force and PFJ contact force. A single stance phase of the motion cycle was divided into eleven time points (periods 0.0-1.0). The computational results were statistically tested at each time point.

Results: The results showed that central ACL reconstruction reduced graft force at contralateral toe-off and toe-off phases under walking conditions and the entire cycle under running conditions, with maximal reductions were 10.96 ± 7.42 % and 29.00 ± 10.41 %, respectively. Compared to AM reconstruction, central reconstruction increased the mean PFJ contact force by up to 2.12 ± 1.17 % of body weight during periods 0.4-0.9 of the walking cycle and exhibited a complex pattern during the running cycle.

Conclusions: Central ACL reconstruction provided a significantly higher PFJ load compared with AM reconstruction during walking after surgery. No consistent conclusions were reached between the two surgical protocols on PFJ contact force during running. These findings provide clinicians with a better understanding of the PFJ mechanics after ACL reconstruction.

Keywords: ACL reconstruction; patellofemoral joint; osteoarthritis; musculoskeletal model; biomechanics

1. Introduction

Patellofemoral joint (PFJ) osteoarthritis (OA) following anterior cruciate ligament (ACL) reconstruction has received much attention in recent years. Clinical studies have reported that 17.4 % of patients developed new-onset PFJ OA after ACL reconstruction [34]. The prevalence of radiographic PFJ OA post-surgery ranges from 11 % to 90 % [13]. Adverse symptoms, such as prepatellar pain caused by cartilage degradation, gravely affect surgical outcomes. Furthermore, young patients would suffer premature joint ageing, which results in an inability to return to sports [14].

Mechanical disorders are among the mechanisms contributing to OA [24]. Cartilage requires sufficient load to maintain its typical structure and function. PFJ underloading appears in various dynamic tasks early after ACL reconstruction, including walking, single-leg hop and running [48], [49], [57]. Recent studies have indicated that reduced PFJ loading in the early stage after surgery is closely associated with poor long-term cartilage and PFJ OA [41], [45], [56]. Consequently, restoring early PFJ mechanics post-ACL reconstruction could be critical in mitigating PFJ degeneration.

Determining the surgical protocol to better restore joint contact is beneficial for promoting cartilage health. Previous research has demonstrated that anatomic double-bundle ACL reconstruction more accurately restores PFJ contact areas and pressures compared to non-anatomic single-bundle reconstruction [50]. With evolving concepts, anatomic single-bundle ACL reconstructions are increasingly used and have achieved clinical outcomes comparable to double-bundle ACL reconstructions [2]. Since anatomic single-bundle ACL reconstructions cannot fully restore the original surface area of the native footprint, the femoral tunnel could be positioned centrally, anteromedially, or posterolaterally within the footprint. Anteromedial (AM) and central ACL reconstructions have proven superior to posterolateral reconstruction for graft isometric, maturation, and knee stabilization [12], [35], [38], [43] and were the two most commonly used reconstruction techniques. Different tunnel placements of the two techniques change the graft angle connecting the femur and tibia. Previous study identified graft angle as a primary determinant of internal knee mechanics after ACL reconstruction [55]. However, biomechanical results of PFJ were not included in this study. To date, the effect of AM and central ACL reconstructions on PFJ contact mechanics remains unclear.

Shreds of evidence have shown that variations in muscle load could also affect TFJ kinematics, further changing the PFJ contact pressures [36], [54]. Therefore, a primary challenge in assessing the potential impact of the surgical protocols on PFJ biomechanics is eliminating the influence of muscle load. Lower limb muscle atrophy is universal in the early stage after ACL reconstruction, which may exacerbate the impact of graft angle on PFJ load under dynamic conditions [9], [42]. Musculoskeletal (MSK) models have advantages in simulating muscle atrophy and dynamic activity under physiological conditions.

Hence, this study used MSK models to determine the effects of AM and central graft tunnel placements on PFJ contact mechanics during walking and running post-anatomic single-bundle ACL reconstruction. First, the kinematics of the TFJ and PFJ of the normal knee during the entire gait cycle were calculated and compared to the experimental studies to verify the MSK model effectiveness. Then, muscle force pre- and post-muscle volume reduction during the gait stance phase was calculated to evaluate the impact of volume changes on muscle force. Finally, graft forces and PFJ contact forces in AM and central ACL reconstructions during the stance phase of both walking and running cycles were calculated and compared. The results were expected to expand biomechanical evidence of ACL reconstruction, and provide potential value for clinicians to optimize rehabilitation strategies after surgery. We hypothesized that PFJ mechanics in AM reconstructed knees would differ from those in central reconstructed knees and that central ACL reconstruction would more effectively restore early PFJ biomechanics post-surgery under dynamic conditions.

2. Methods

2.1 Subject information

Motion capture data and ground reaction force (GRF) of walking trials [18] and running trials [19] were obtained from two public databases. All subjects from the databases were healthy without any neurological or musculoskeletal disorder. The subjects were asked to perform walking or running trials on an instrumented treadmill comfortably. A three-dimensional (3D) motion-capture system with 12 cameras was used to collect kinematics. Detailed information of selected subjects was shown in Table 1.

Table 1. Details of the subjects involved in the current study.

Walking				Running			
	Height (m)	Weight (kg)	Speed (m/s)		Height (m)	Weight (kg)	Speed (m/s)
Subject 1	1.79	75.85	1.27	Subject 7	1.80	75.00	2.5
Subject 2	1.67	52.90	1.25	Subject 8	1.66	56.85	2.5
Subject 3	1.70	62.45	1.28	Subject 9	1.69	60.00	2.5
Subject 4	1.71	61.15	1.32	Subject 10	1.72	64.70	2.5
Subject 5	1.86	79.05	1.16	Subject 11	1.83	80.00	2.5
Subject 6	1.76	66.25	1.21	Subject 12	1.75	68.15	2.5

2.2 MSK modelling

2.2.1 Description of model

Lower limb models were developed utilizing AnyBody (v7.4, AnyBody Technology, Denmark) [15]. The lower limb MSK model was taken from the AnyBody Managed Model Repository (v2.2.1) and modified for this study [31]. Fifty-five muscle-tendon units comprised of roughly 160 three-element Hill-type muscle models actuated the model.

2.2.2 Model scaling

The segments and isometric muscle strength of each muscle model were scaled via a length-mass-fat scaling approach according to the height and weight of subjects [26]. Moreover, a parameter optimization method proposed by Andersen et al. [1] was also used to scale the skeleton and determine the joint center.

2.2.3 Geometry of bone and cartilage

Six normal right knee joint models comprising bones (femur, tibia, and patella) and articular cartilage (femoral cartilage, medial and lateral tibial cartilage, and patellar cartilage) were included in the current study. The 3D geometric surfaces were sourced from Open Knee, a publicly available project, have been previously verified [11]. Detailed information of all models was shown in Table 2. The models were selected to match the motion capture data according to the most similar body mass index (BMI) of the subjects. The mean absolute difference of BMI in walking and running trials was 0.45 ± 0.45 and 1.13 ± 0.72, respectively.

Two-sample t tests were used to determine the significance of the differences. No significant differences of BMI in both walking trials (P = 0.736) and the running trials (P = 0.322) after the matching step. Then, the knee joint models were integrated into the MSK models via rigid registration, performed in Geomagic Studio (v2013, Geomagic Inc., USA). The bone registration was implemented by aligning the bony landmarks of femur (lateral and medial epicondyle, apex of intercondylar notch, trochlea groove), tibia (lateral and medial edge of tibial plateau, tibial tuberosity) and patella (lateral and medial border, base and apex of patella) between the geometric surfaces of knee joint models and MSK models. The registration of cartilages was performed an automatic alignment according to the transform matrixes of the attached bone, respectively.

Table 2. Details of the models included in the current study.

ID	oks001	oks002	oks004	oks006	oks007	oks008
Side	Right	Right	Right	Right	Right	Right
Height (m)	1.83	1.55	1.58	1.52	1.70	1.78
Weight (kg)	77.1	45.3	54.4	49.4	65.8	63.5
BMI	23.1	18.9	21.9	21.3	22.7	20.1

2.2.4 Ligament bundle

Eighteen non-linear one-dimensional spring ligament bundles were modelled around the TFJ and PFJ to maintain stability during physiological motion simulation: anteromedial (aACL) and posterolateral (pACL) bundles of the anterior cruciate ligament; anterolateral (aPCL) and posteromedial (pPCL) bundles of the posterior cruciate ligament; lateral collateral ligament (LCL); anterior portion (aMCL), central portion (cMCL) and posterior portion (pMCL) of the medial collateral ligament; medial (Mcap) and lateral (Lcap) posterior capsules; oblique popliteal ligament (OPL); superior (sMPFL), middle (mMPFL) and inferior (iMPFL) medial PF ligament; superior (sLPFL), middle (mLPFL) and inferior (iLPFL) lateral PF ligament and patellar tendon (PT) (Fig. 1A). The 3D coordinates of the ligament bundle attachment points were obtained from subject-specific MR images. Wrapping surfaces were applied to the ligament bundles to wrap around the bony structure to prevent ligament penetration into the bone.

The force-strain relationship of the non-linear spring ligaments was defined as follows [7]:

$$f(\varepsilon) = \begin{cases} k(\varepsilon - \varepsilon_1), & 2\varepsilon_1 < \varepsilon \\ \frac{k\varepsilon^2}{4\varepsilon_1}, & 0 \le \varepsilon \le 2\varepsilon_1 \\ 0, & \varepsilon < 0 \end{cases} \tag{1}$$

$$\varepsilon = \frac{l - l_0}{l_0} \tag{2}$$

where $f(\varepsilon)$ is the current force, k is the stiffness, ε is the strain, and ε_1 is assumed to be constant at 0.03. l_0 is the ligament bundle zero-load length. Two methods were used to determine the ligament bundle zero-load length; one is the zero-load length percentage method, which considered to take subject-specific ligament information into account [8]:

$$l_0 = l_{max} \times CPCT \tag{3}$$

where $l_{\max}$ is the maximum length of the ligament bundle in passive knee flexion, and CPCT is the correction percentage. This method was applied to determine the l_0 of ACL, PCL, MCL and LCL. The $l_{\max}$ of each ligament was converted by the length at the extended position using the length change pattern [3]. The best CPCT were the cruciates (ACL and PCL) at 85 % and the collaterals (LCL and MCL) at 75 %, according to the literature [8]. Another is the reference strain method:

$$l_0 = \frac{l_r}{\varepsilon_r + 1} \tag{4}$$

where l_r is the ligament reference length at the reference (extension) position, and ε_r is the ligament reference strain at the reference position. This method was applied to determine the l_0 other than ACL, PCL, MCL and LCL. The l_0 of the PT was measured from sagittal MRI images. The stiffness and reference strain values of the ligament bundle could be found in previous literature [6], [39].

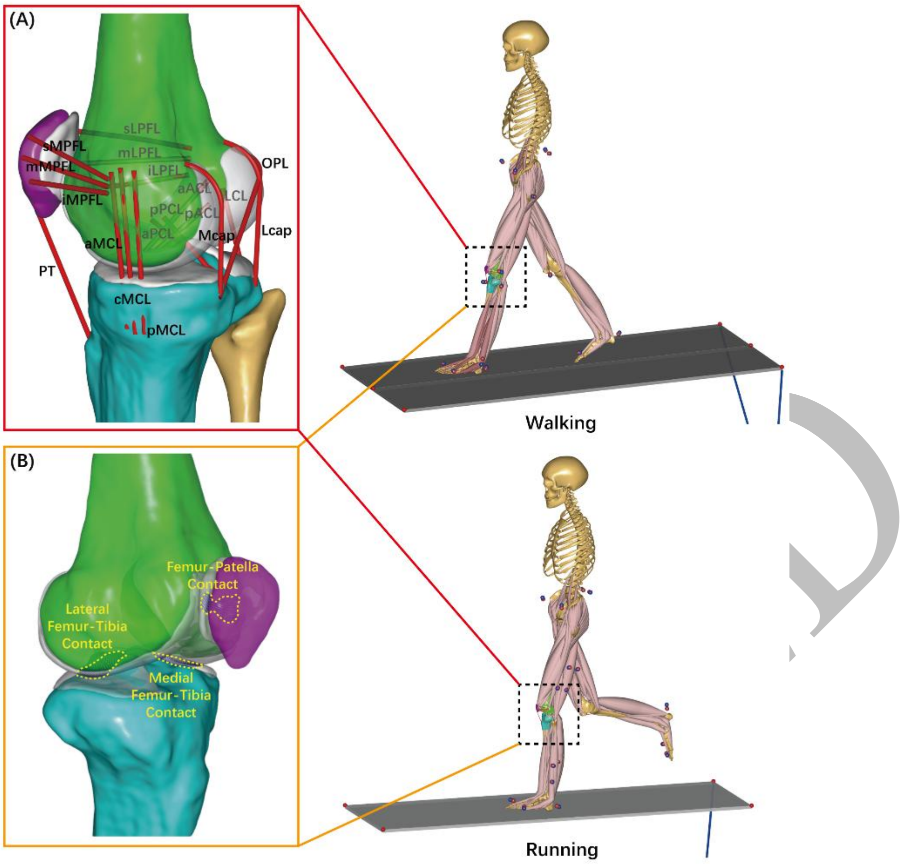

Fig. 1. Subject-specific musculoskeletal model during walking and running conditions. (A) Eighteen ligament bundles. (B) Contact conditions between femur, tibia and patella.

2.2.5 Contact conditions

Three rigid-rigid STL-based contact pairs were defined between the femoral and tibial cartilage and between the femoral and patellar cartilage (Fig. 1B). The contact surface was defined as the entire cartilage area, and the two opposite surfaces were in a master-slave relationship. All contact surfaces were represented with the triangles of the STL files. The contact forces of each contact pair were computed using a linear force-penetration volume law [6]. One vertex of the triangular meshes penetrates the opposite surface, forming a penetration depth (the distance between the vertex and the nearest point on the opposite surface) and a contact area (one-third of the sum of the areas of adjacent triangles). The penetration volume was the product of the penetration depth and the contact area. A pressure module of 1.2E10 N/m^3 was applied to determine contact force magnitudes at cartilaginous interfaces [28]. The vertex contact force was the product of the penetration volume and the pressure module. The contact force for each contact pair was the vector sum of all the vertex contact forces.

2.2.6 Definition of TFJ and PFJ

A joint coordinate system (CS) was defined to describe the kinematics for both the TFJ and PFJ according to previous studies [10], [16]. The kinematics of TFJ and PFJ were described as the tibia with respect to the femur and the patella with respect to the femur, respectively. The 3D translation was measured by the relative displacement between the origins of the two CSs. Angular rotations were calculated using a Cardan angle in the following sequences: flexion-extension, abduction-adduction and external-internal rotation for TFJ [25] and flexion, rotation and tilt for PFJ [16].

2.2.7 Simulation of the AM and central ACL reconstructions

The aACL and pACL ligament bundles of the normal knee joint models were removed and subsequently reconstructed (Fig. 2A). Attachment points for the femur and tibia were determined based on prior research employing the quadrant method [4], [53]. The numerical description of the femoral tunnel was measured based on a sagittal plane grid aligned to the Blumensaat line. The numerical description of the tibial tunnel was measured based on an axial plane grid with the transverse line (defined by the most posterior margin of the lateral and medial tibial condyles) aligned to the coronal plane. Grids were constructed using SolidWorks (v2018, Dassault Systemes, USA) by an experienced researcher. The AM femoral tunnel placement was 23.7 % depth and 21.3 % height. The center femoral tunnel placement was 28.2 % depth and 34.8 % height [59] (Fig. 2B). The tibial tunnel placement was 46.1 % anterior and 47.6 % medial [51] (Fig. 2C). The stiffness of the reconstructed ACL graft was set as the product of the normal ACL stiffness used in MSK model [6] and the actual stiffness ratio of the normal ACL [58] and the double-looped semitendinosus and gracilis graft [27].

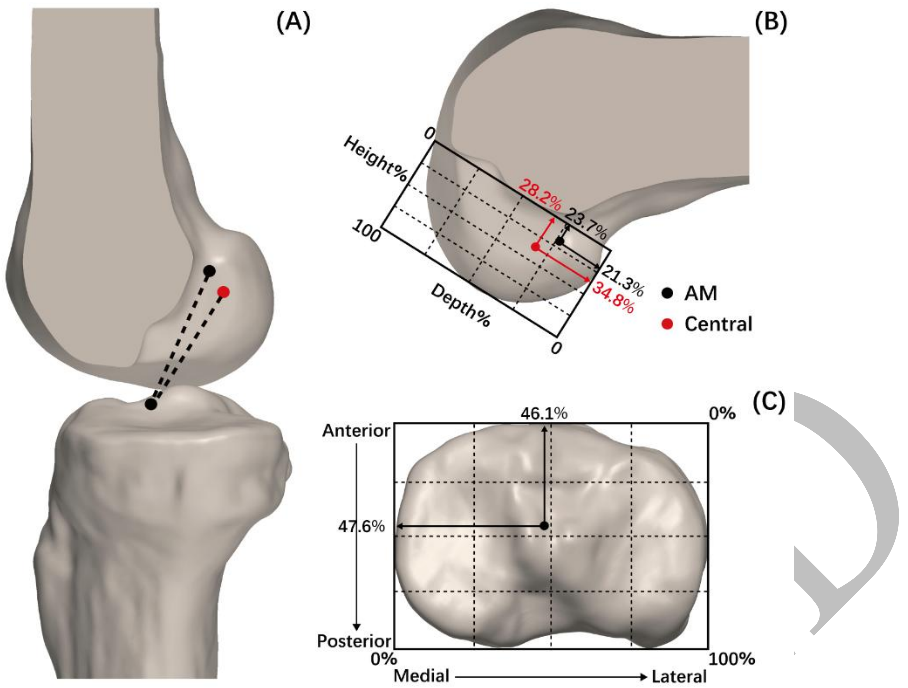

Fig. 2. Subject-specific ACL reconstruction models (A) Schematic of the AM and central ACL reconstruction. (B) The AM and central femoral tunnel placement were defined using the quadrant method. (C) The tibial tunnel placement was defined using the quadrant method.

2.2.8 Simulate muscle atrophy

Quadriceps femoris and hamstrings muscle volumes were modified based on an MR-based quantitative study to accurately model muscle force post-ACL reconstruction [40]. The ratio of postoperative to normal muscle volume was applied to the rectus femoris (RF: 78.26 %), vastus lateralis (VL: 74.29 %), vastus medialis (VM: 80 %), vastus intermedius (VI: 78.26 %) and semitendinosus (ST: 83.33 %). As a result, each muscle force was adjusted and resolved to achieve balance during motion simulation.

2.2.9 Inverse kinematics and dynamic analysis

An inverse kinematics method based on motion capture data was employed to track the marker trajectories during one motion cycle [1]. The entire gait cycle was defined from heel-strike to next heel-strike. The stance phase of both walking and running cycles was defined from heel-strike to toe-off. A GRF threshold of 10 N was used to define heel-strike and toe-off. Following the kinematic analysis, inverse dynamics analysis, including force-dependent kinematics (FDK) solver, was performed [47]. During the FDK-solving process, muscle forces, secondary joint kinematics, ligament forces and joint contact forces were calculated. All simulation results were resampled on a 0-100 % trial duration scale at 1 % intervals. Both muscle force and joint contact force were normalized by body weight (BW).

2.3 Statistical analysis

Differences between model calculations and in vivo experimental measurements reported by Gary et al. [23] were quantified using interclass correlation coefficient (ICC) of type (3,1) according to Shrout and Fleiss [46]. An ICC > 0.75 indicates excellent, 0.75-0.40 moderate to good and < 0.40 poor reliability [22]. A single stance phase of the walking and running cycles was divided into eleven-time points (periods 0.0-1.0). The calculated graft forces and PFJ contact forces in each model were compared with the corresponding simulation data from the same knee at the same cycle phase. The Shapiro-Wilk test was used to detect data normality. If the data conformed to the normality, paired t-tests were performed to detect statistically significant differences in the AM and central ACL reconstruction data. The Wilcoxon signed-rank test was used if the data did not conform to normality. To account for multiple testing, *P* values were adjusted according to the method of Holm-Bonferroni to control the family-wise error rate. All analyses were performed using SPSS (v19.0, IBM Statistics, New York, USA). Cohen's *d* was reported as the effect size, with the following interpretation standards: 0.8 (large), 0.5 (medium), and 0.2 (small) [44]. In addition, continuous analysis of time series data through Statistical Parametric Mapping (SPM) was also performed. SPM two-sample independent t-tests ($P < 0.05$) were used to compare the results between groups. All analyses were implemented using the open-source spm1d code on Python software (v7.2).

3. Results

3.1 Comparison of TFJ and PFJ kinematics in intact model

Predicted versus experimental [23] 6-DOF kinematics of the TFJ and sagittal kinematics of PFJ during the entire gait cycle are depicted in Fig. 3. The established MSK models can reasonably predict the overall trend of kinematics and the characteristic peak value of the TFJ and PFJ during the gait cycle (Table 3). The inter-session reliability for flexion, valgus in TFJ and anterior, superior translation in PFJ were excellent, with ICC of 0.766, 0.835, 0.924, 0.803 and confidence interval of 95 % from 0.671-0.836, 0.764-0.885, 0.889-0.948, 0.721-0.869, respectively. The inter-session reliability for the other kinematics in TFJ and PFJ was moderate to good.

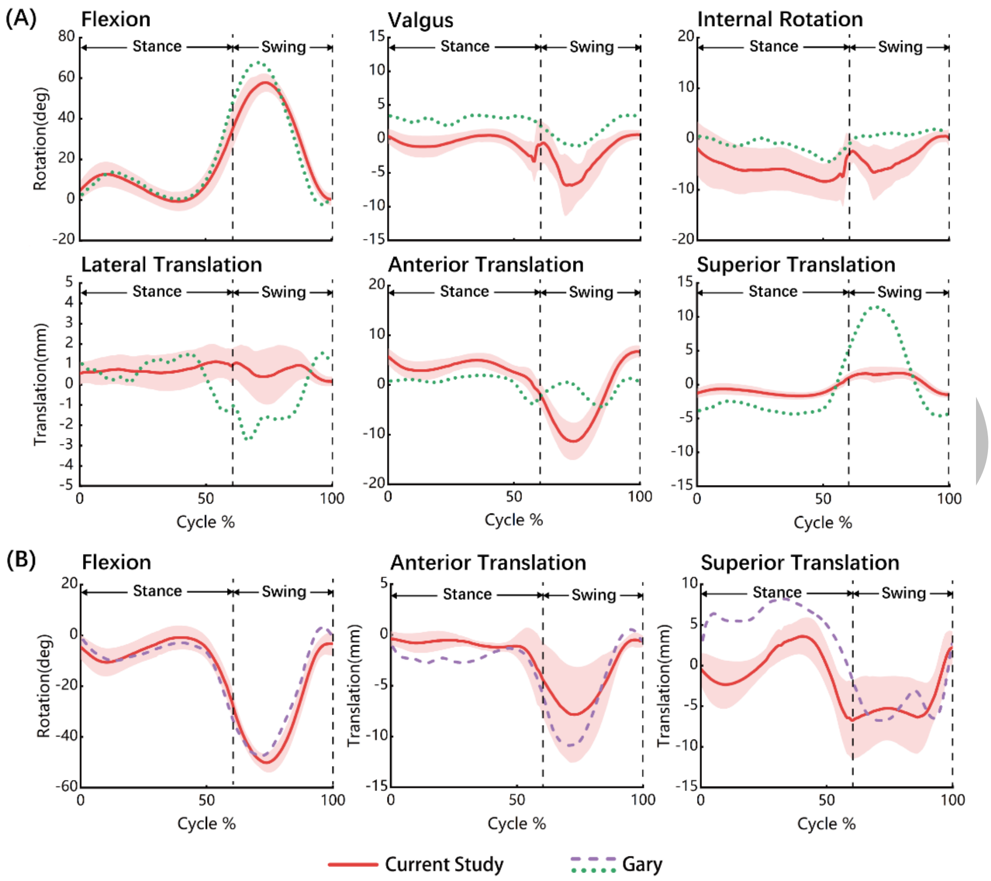

Fig. 3. (A) The 6-DOF tibiofemoral joint kinematics describing displacements of the tibia with respect to the femur for one entire gait cycle. (B) The sagittal kinematics of patellofemoral joint kinematics describing displacements of the patella with respect to the femur for one entire gait cycle. (The positive direction of the three rotational DOFs [47] was opposite to the current study)

Table 3. Agreement between predicted and in vivo experimental 6-DOF kinematics of TFJ (A) and sagittal kinematics of PFJ (B) during the entire gait cycle.

(A)	Flexion	Valgus	Internal Rotation	Lateral Translation	Anterior Translation	Superior Translation
ICC	0.766	0.835	0.722	0.474	0.411	0.538
95% CI	0.671-0.836	0.764-0.885	0.614-0.804	0.220-0.645	0.236-0.561	0.315-0.689

(B)	Flexion	Anterior Translation	Superior Translation
ICC	0.688	0.924	0.803

95% CI	0.569-0.778	0.889-0.948	0.721-0.869

ICC: interclass correlation coefficient

CI: confidence interval

3.2 Prediction of muscle force

The mean muscle forces of the RF and ST continued to be lower than normal after reducing muscle volume (Fig. 4). The peak force of the RF was 0.48 BW, decreasing by 22.58 % compared to the normal value of 0.62 BW, occurring at the contralateral heel-strike of the stance phase. The mean peak muscle force of the ST was 0.20 BW, decreasing by 20.00 % compared to the normal value of 0.25 BW, occurring at the heel strike of the stance phase. The mean muscle force of the VL was lower than normal before the 0.6 periods and then higher than normal. The peak force was 0.36 BW, decreasing by 7.69 % compared to the normal value of 0.39 BW, occurring at the contralateral toe-off of the stance phase. The mean muscle forces of the VM and VI increased slightly toward the end of the stance phase. The peak forces were 0.10 BW and 0.04 BW, respectively, almost the same as normal, occurring at the contralateral toe-off of the stance phase. The above results showed the necessity of muscle volume modification in post-operative dynamic activity simulation using kinematic data of healthy subjects.

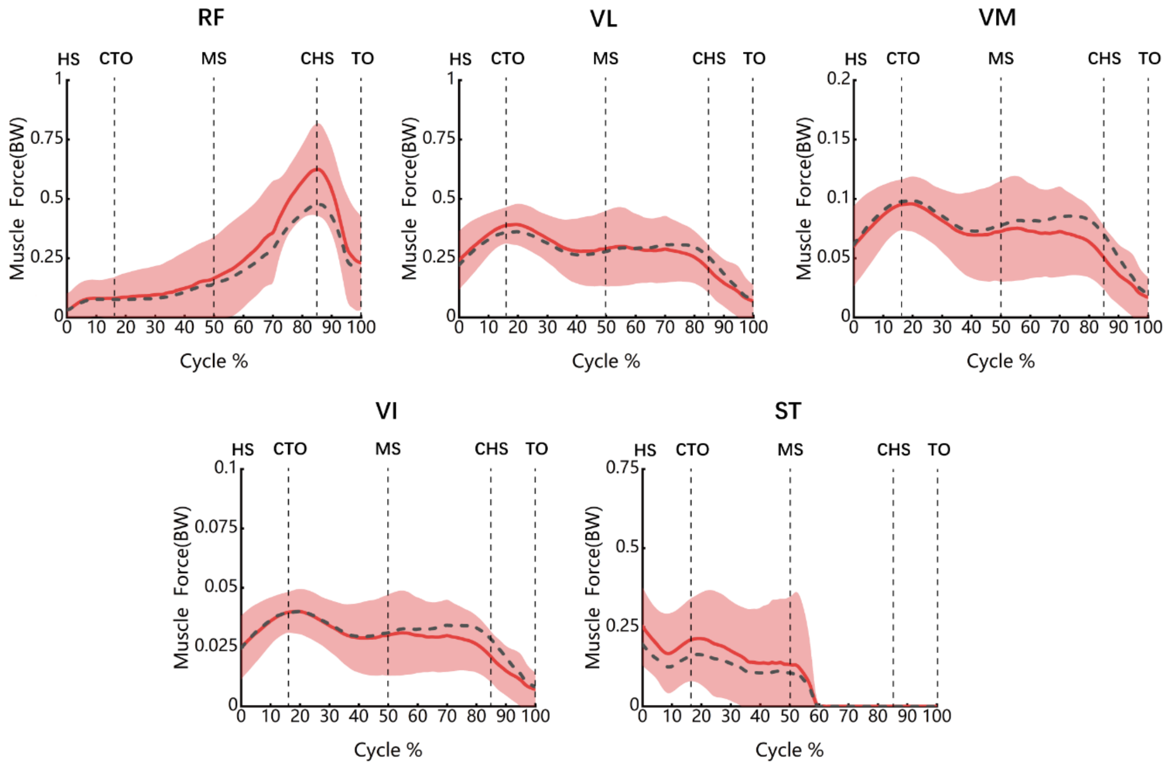

Fig. 4. Mean muscle forces predicted before and after muscle volume reduction during the stance phase of gait. Solid lines represent a normal muscle volume, and dashed lines represent a decreased muscle volume. (RF, rectus femoris; VL, vastus lateralis; VM, vastus medialis; VI, vastus intermedius; ST, semitendinosus; HS, heel-strike; TO, toe-off; CTO, contralateral toe-off; MS, midstance; CHS, contralateral heel-strike)

3.3 Graft force

Results show that forces exerted on the ACL graft during the stance phase of the walking and running cycles, see Figure 5. Compared with AM reconstruction, the mean force on ACL graft of central reconstruction was reduced by 9.06 ± 7.31 % in the 0.2 period near the contralateral toe-off of the stance phase, under the walking-load condition. At the toe-off of the stance phase, the mean force on the ACL graft of central reconstruction was reduced by 10.96 ± 7.42 %, compared with AM reconstruction. Under the running-load condition, the mean force on the ACL graft of central reconstruction remained lower than AM reconstruction throughout the stance phase of running. The peak graft force was reduced by 29.00 ± 10.41 % in the 0.3 period. Fig. 6A and Fig. 6B show the comparisons of the graft forces-time series by SPM under walking and running conditions, respectively. Nonsignificant ($P > 0.05$) differences between all pairwise comparisons.

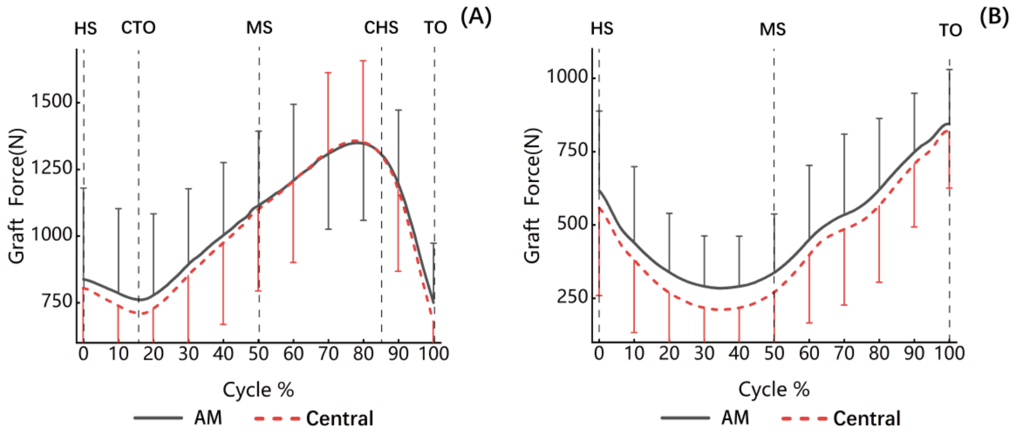

Fig. 5. Comparison between the AM and central ACL reconstruction of the forces exerted on the ACL grafts during the stance phase of the walking (A) and running (B) cycle. (HS, heel-strike; TO, toe-off; CTO, contralateral toe-off; MS, midstance; CHS, contralateral heel-strike)

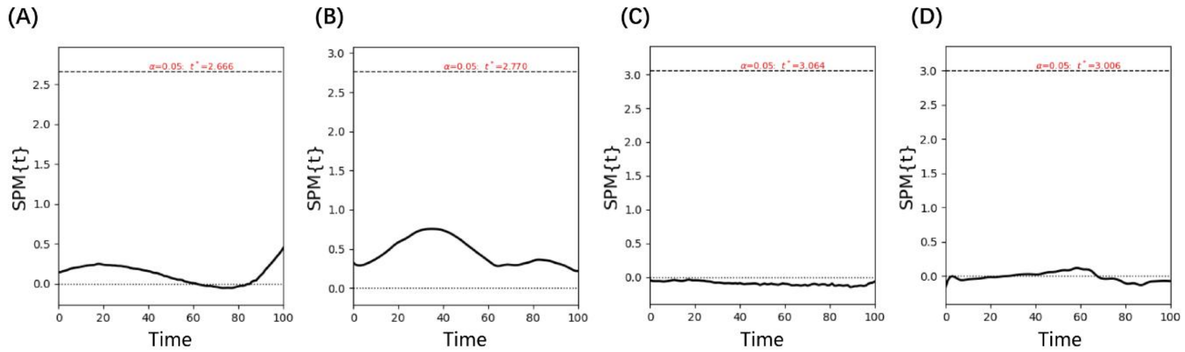

Fig. 6. Comparison of graft forces/patellofemoral joint contact forces-time series by SPM between reconstruction types. (Graft forces during the stance phase of the (A) walking and (B) running; Patellofemoral joint contact forces during the stance phase of the (C) walking and (D) running)

3.4 PFJ Contact Force

The PFJ contact forces during the stance phase of the walking and running cycles are depicted in Fig. 7. Compared with AM reconstruction, the mean PFJ contact force of central reconstruction was significantly increased under the walking-load condition by 1.06 ± 0.39 %BW (P = 0.006, Cohen's d = 0.059), 1.62 ± 0.60 %BW (P = 0.001, Cohen's d = 0.065), 1.60 ± 0.88 %BW (P = 0.001, Cohen's d = 0.062), 2.12 ± 1.17 %BW (P = 0.002, Cohen's d = 0.078), 1.83 ± 0.62 %BW (P = 0.001, Cohen's d = 0.073) and 1.79 ± 0.49 %BW (P < 0.001, Cohen's d = 0.091), respectively, in the 0.4, 0.5, 0.6, 0.7, 0.8 and 0.9 periods. Compared with AM reconstruction, the mean PFJ contact force of central reconstruction was increased in the

0.0-0.2 periods, and then reduced in the 0.3-0.6 periods, and finally increased in the 0.7-1.0 periods, under the running-load condition. However, these differences were not statistically significant. In addition, it was worth noting that although the two graft conditions caused statistical differences of PFJ contact forces at several time points in the walking cycle, this might not be meaningful and clinically relevant due to the small effect sizes of the results. Fig. 6C and Fig. 6D show the comparisons of the PFJ contact forces-time series by SPM under walking and running conditions, respectively. Nonsignificant (*P* > 0.05) differences between all pairwise comparisons.

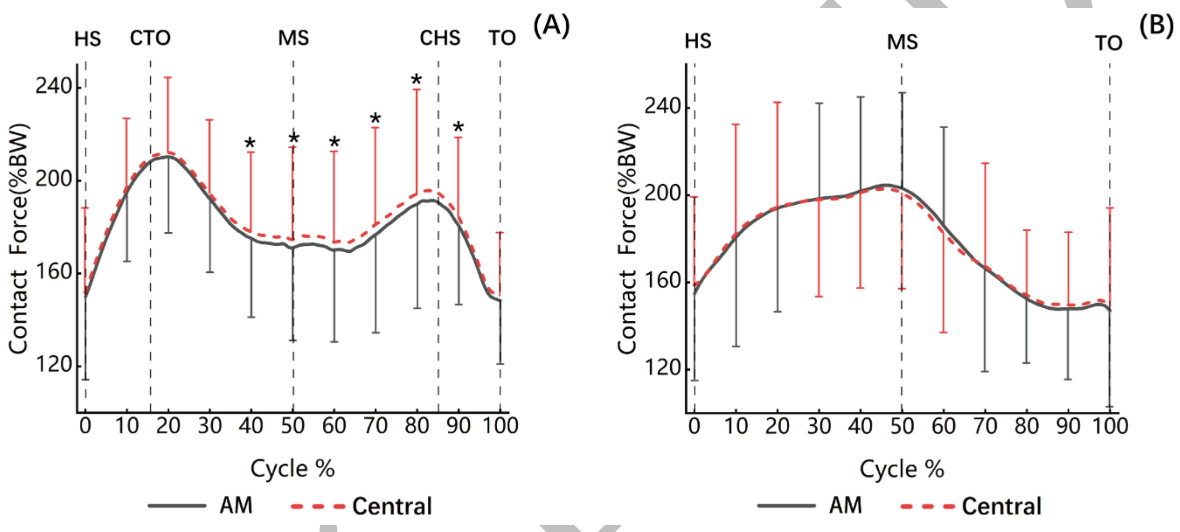

Fig. 7. Comparison between the AM and central ACL reconstruction of the patellofemoral joint contact forces during the stance phase of the walking (A) and running (B) cycle. (* means significant differences; HS, heel-strike; TO, toe-off; CTO, contralateral toe-off; MS, midstance; CHS, contralateral heel-strike)

4. Discussion

This study aims to investigate the effect of AM and central ACL reconstructions on the PFJ contact mechanics during walking and running. The primary finding is that central ACL reconstruction provides a significantly higher PFJ load than AM ACL reconstruction during walking after surgery. The maximum difference is 2.12 ± 1.17 %BW in the 0.7 period. Nevertheless, no consistent conclusions were reached between the two surgical protocols regarding PFJ contact force during running. AM ACL reconstruction provides a higher PFJ contact force in 0.3-0.6 periods, while central ACL reconstruction provides a higher PFJ contact force in 0.0-0.2 and 0.7-1.0 periods during the running cycle.

Articular cartilage is a mechanosensitive tissue. Following ACL tear, the ACL-deficient lower limb has been reported to decrease the PFJ contact forces by approximately 30 % [26]. Simultaneously, osteoarthritic-associated cartilage composition would also reduce [32]. Cyclic joint loads generated by joint motion are essential to maintain normal metabolism and structure of cartilage. However, PFJ load during dynamic activity is often insufficient due to lower limb muscle atrophy and reduced joint mobility after ACL reconstruction [48], [49], [57] which may be the initiating factor leading to long-term PFJ degeneration. In addition, given the weakness of ACL graft soon early after surgery [21], excessive stress should be avoided to avoid secondary tissue damage. Therefore, PFJ loads closed to pre-injury conditions and lower graft forces are considered advantageous when evaluating the impact of the ACL reconstruction surgical protocol on PFJ biomechanics under dynamic conditions.

Previous studies reported that peak PFJ contact forces of the ACL reconstructed limb averagely decreased by 0.2-0.4 BW (20-40 %BW) and 0.6 BW (60 %BW) during walking and running, respectively, compared with the uninjured limb within 24 months after surgery [57], [49]. The threshold of these findings was much greater than that of the current study, meaning that the differences in PFJ contact forces caused by two surgical interventions, while significant, might not be clinically relevant. Few studies have indicated no differences in clinical outcomes between AM and central ACL reconstruction [59], which supported this hypothesis to some extent. Further research is needed to confirm the significance of the current findings in PFJ degeneration after ACL reconstruction.

The ACL graft acts as a stabilizer connecting the femur and tibia, further affecting the PFJ contact mechanics by affecting the TFJ kinematics. A previous biomechanical study has demonstrated that increased tibial posterior translation and external rotation could result in higher PFJ contact pressure in normal knee joints [36]. Another study also indicated that excessive posterior tibial loading during ACL reconstruction increased PFJ contact pressures at the time of surgery [29]. The native ACL fibers close to the femoral footprint location of AM reconstruction have been proven to mainly resist anterior tibial translation [30]. In the current study, the ACL graft forces of AM reconstruction were significantly greater than those of central reconstruction in both walking and running cycles, consistent with the previous findings. In addition, a simulation study revealed that a more vertical ACL graft induced greater anterior tibial translation, internal rotation and ACL loading in walking conditions [55]. The above results may explain why AM ACL reconstruction results in lower PFJ loading than central ACL reconstruction.

Lower limb muscle force, especially the quadriceps femoris, is essential in the mechanics of the PFJ during dynamic load conditions [5]. In vivo ACL strain increases concurrently with quadriceps femoris force [17], which means that the quadriceps femoris force and the ACL graft tension may be synergetic factors in PFJ mechanics. Clinical studies found that quadriceps femoris dysfunction is common in patients with PFJ degeneration [33]. The atrophy degree of each quadriceps femoris muscle was different, and the duration of atrophy and recovery were also different after ACL reconstruction [9]. Unbalanced atrophy of the quadriceps femoris could affect the static alignment of the PFJ and has been confirmed to be associated with PFJ degeneration [37]. Additionally, the current study showed that muscle forces changed differently after reduced muscle volume, emphasizing the necessity of modifying muscle volume in investigating PFJ biomechanics during dynamic activity after ACL reconstruction. In vitro cadaver experiments present with challenges in accurately loading muscle forces in a state of muscle atrophy. In contrast, MSK models have advantages in predicting in vivo joint contact forces and muscle forces during physiological activities [28], [52].

Several limitations of this study should be noted. First, only walking and running activities were included in this study. Other functional activities in daily life, such as step-ups, lunges and squats, should be considered. Secondly, the current study considered only the atrophy of the quadriceps femoris and hamstrings, whereas muscle atrophy is more extensive after ACL reconstruction. Fixed atrophy ratios were used without validation against longitudinal patient data, which may affect the generalizability of the results. Third, only the sagittal kinematics of the PFJ and the 6-DOF kinematics of the TFJ were reported during model validation because the PFJ contact forces were mainly affected by the above factors after ACL reconstruction. Due to the lack of individual data points in the compared experimental study, the absolute errors were not reported in the current research, which limited validation of the results to some extent. In addition, there is biomechanical asymmetry in the involved limb compared with the uninvolved limb after ACL reconstruction. Individuals with ACL reconstruction walk with a stiffer knee throughout the stance [20], which will change the movement trajectory and GRF. However, this study did not take this into account.

5. Conclusion

The study concluded that central ACL reconstruction provided a significantly higher PFJ load compared with AM reconstruction during walking, which might be conducive to early PFJ biomechanics after surgery. No consistent conclusions were reached between the two surgical protocols on PFJ contact force during running. The results from this study may help clinicians better understand the PFJ mechanics after ACL reconstruction. More clinical studies and patient-based longitudinal biomechanical analyses are required in the future to confirm the conclusions of this study.

Conflicts of interest

The authors declare that they have no conflict of interest.

Acknowledgements

This study was sponsored by the National Natural Science Foundation of China (Grant No. 12272164).

References

1. ANDERSEN M.S., DAMSGAARD M., MACWILLIAMS B., RASMUSSEN J., *A computationally efficient optimisation-based method for parameter identification of kinematically determinate and over-determinate biomechanical systems*, Comput Methods Biomech Biomed Engin, 2010, 13(2), 171-183.
2. BALASINGAM S., KARIKIS I., ROSTGÅRD-CHRISTENSEN L., DESAI N., AHLDÉN M., SERNERT N., KARTUS J., *Anatomic Double-Bundle Anterior Cruciate Ligament Reconstruction Is Not Superior to Anatomic Single-Bundle Reconstruction at 10-Year Follow-up: A Randomised Clinical Trial*, Am J Sports Med, 2022, 50(13), 3477-3486.
3. BELVEDERE C., ENSINI A., FELICIANGELI A., CENNI F., D'ANGELI V., GIANNINI S., LEARDINI A., *Geometrical changes of knee ligaments and patellar tendon during passive flexion*, J Biomech, 2012, 45(11), 1886-1892.

4. BERNARD M., HERTEL P., HORNUNG H., CIERPINSKI T., *Femoral insertion of the ACL. Radiographic quadrant method*, Am J Knee Surg, 1997, 10(1), 14-21.
5. BESIER T.F., FREDERICSON M., GOLD G.E., BEAUPRÉ G.S., DELP S.L., *Knee muscle forces during walking and running in patellofemoral pain patients and pain-free controls,* J Biomech, 2009, 42(7), 898-905.
6. BLANKEVOORT L., KUIPER J.H., HUISKES R., GROOTENBOER H.J., *Articular contact in a three-dimensional model of the knee*, J Biomech, 1991, 24(11), 1019-1031.
7. BLANKEVOORT L., HUISKES R., *Ligament-bone interaction in a three-dimensional model of the knee,* J Biomech Eng, 1991, 113(3), 263-269.
8. BLOEMKER K.H., GUESS T.M., MALETSKY L., DODD K., *Computational knee ligament modeling using experimentally determined zero-load lengths*, Open Biomed Eng J, 2012, 6, 33-41.
9. CAI W.S., LI H.H., KONNO S.I., NUMAZAKI H., ZHOU S.Q., ZHANG Y.B., HAN G.T., *Patellofemoral MRI Alterations Following Single Bundle ACL Reconstruction with Hamstring Autografts Are Associated with Quadriceps Femoris Atrophy*, Curr Med Sci, 2019, 39(6), 1029-1036.
10. CARBONE V., FLUIT R., PELLIKAAN P., VAN DER KROGT M.M., JANSSEN D., DAMSGAARD M., VIGNERON L., FEILKAS T., KOOPMAN H.F., VERDONSCHOT N., *TLEM 2.0 - a comprehensive musculoskeletal geometry dataset for subject-specific modeling of lower extremity*, J Biomech, 2015, 48(5), 734-741.
11. CHOKHANDRE S., SCHWARTZ A., KLONOWSKI E., LANDIS B., ERDEMIR A., *Open Knee(s): A Free and Open Source Library of Specimen-Specific Models and Related Digital Assets for Finite Element Analysis of the Knee Joint*, Ann Biomed Eng, 2023, 51(1), 10-23.
12. CROSS M.B., MUSAHL V., BEDI A., O'LOUGHLIN P., HAMMOUD S., SUERO E., PEARLE A.D., *Anteromedial versus central single-bundle graft position: which anatomic graft position to choose?* Knee Surg Sports Traumatol Arthrosc, 2012, 20(7), 1276-1281.
13. CULVENOR A.G., COOK J.L., COLLINS N.J., CROSSLEY K.M., *Is patellofemoral joint osteoarthritis an under-recognised outcome of anterior cruciate ligament reconstruction? A narrative literature review*, Br J Sports Med, 2013, 47(2), 66-70.

14. CULVENOR A.G., LAI C.C., GABBE B.J., MAKDISSI M., COLLINS N.J., VICENZINO B., MORRIS H.G., CROSSLEY K.M., *Patellofemoral osteoarthritis is prevalent and associated with worse symptoms and function after hamstring tendon autograft ACL reconstruction*, Br J Sports Med, 2014, 48(6), 435-439.
15. DAMSGAARD M., RASMUSSEN J., CHRISTENSEN S.T., SURMA E., DE ZEE M., *Analysis of Musculoskeletal Systems in the Anybody Modeling System*, Simul Model Pract Theory, 2006, 14(8), 1100-1111.
16. DZIALO C.M., PEDERSEN P.H., JENSEN K.K., DE ZEE M., ANDERSEN M.S., *Evaluation of predicted patellofemoral joint kinematics with a moving-axis joint model*, Med Eng Phys, 2019, 73, 85-91.
17. ENGLANDER Z.A., FOODY J.N., CUTCLIFFE H.C., WITTSTEIN J.R., SPRITZER C.E., DEFRATE L.E., *Use of a Novel Multimodal Imaging Technique to Model In Vivo Quadriceps Force and ACL Strain During Dynamic Activity*, Am J Sports Med, 2022, 50(10), 2688-2697.
18. FUKUCHI C.A., FUKUCHI R.K., DUARTE M., *A public dataset of overground and treadmill walking kinematics and kinetics in healthy individuals*, PeerJ, 2018, 6, e4640.
19. FUKUCHI R.K., FUKUCHI C.A., DUARTE M., *A public dataset of running biomechanics and the effects of running speed on lower extremity kinematics and kinetics*, PeerJ, 2017, 5, e3298.
20. GARCIA S.A., JOHNSON A.K., BROWN S.R., WASHABAUGH E.P., KRISHNAN C., PALMIERI-SMITH R.M., *Dynamic knee stiffness during walking is increased in individuals with anterior cruciate ligament reconstruction*, J Biomech, 2023, 146, 111400.
21. GORADIA V.K., ROCHAT M.C., GRANA W.A., ROHRER M.D., PRASAD H.S., *Tendon-to-bone healing of a semitendinosus tendon autograft used for ACL reconstruction in a sheep model*, Am J Knee Surg, 2000, 13(3), 143-151.
22. GOUELLE A., MÉGROT F., PRESEDO A., HUSSON I., YELNIK A., PENNEÇOT G.F., *The gait variability index: a new way to quantify fluctuation magnitude of spatiotemporal parameters during gait*, Gait Posture, 2013, 38(3), 461-465.
23. GRAY H.A., GUAN S., THOMEER L.T., SCHACHE A.G., DE STEIGER R., PANDY M.G., *Three-dimensional motion of the knee-joint complex during normal walking revealed*

by mobile biplane x-ray imaging, J Orthop Res, 2019, 37(3), 615-630.

24. GRIFFIN T.M., GUILAK F., *The role of mechanical loading in the onset and progression of osteoarthritis,* Exerc Sport Sci Rev, 2005, 33(4), 195-200.
25. GROOD E.S., SUNTAY W.J., *A joint coordinate system for the clinical description of three-dimensional motions: application to the knee,* J Biomech Eng, 1983, 105(2), 136-144.
26. HASLER E.M., HERZOG W., *Quantification of in vivo patellofemoral contact forces before and after ACL transection*, J Biomech, 1998, 31(1), 37-44.
27. HAUT DONAHUE T.L., HOWELL S.M., HULL M.L., GREGERSEN C., *A biomechanical evaluation of anterior and posterior tibialis tendons as suitable single-loop anterior cruciate ligament grafts,* Arthroscopy, 2002, 18(6), 589-597.
28. HU J., XIN H., CHEN Z., ZHANG Q., PENG Y., JIN Z., *The role of menisci in knee contact mechanics and secondary kinematics during human walking,* Clin Biomech (Bristol, Avon), 2019, 61, 58-63.
29. HUANG W., ONG M.T., MAN G.C., LIU Y., LAU L.C., YUNG P.S., *Posterior Tibial Loading Results in Significant Increase of Peak Contact Pressure in the Patellofemoral Joint During Anterior Cruciate Ligament Reconstruction: A Cadaveric Study,* Am J Sports Med, 2021, 49(5), 1286-1295.
30. KAWAGUCHI Y., KONDO E., TAKEDA R., AKITA K., YASUDA K., AMIS A.A., *The role of fibers in the femoral attachment of the anterior cruciate ligament in resisting tibial displacement,* Arthroscopy, 2015, 31(3), 435-444.
31. KLEIN HORSMAN M.D., KOOPMAN H.F., VAN DER HELM F.C., PROSÉ L.P., VEEGER H.E., *Morphological muscle and joint parameters for musculoskeletal modelling of the lower extremity,* Clin Biomech (Bristol, Avon), 2007, 22(2), 239-247.
32. KLOCKE N.F., AMENDOLA A., THEDENS D.R., WILLIAMS G.N., LUTY C.M., MARTIN J.A., PEDERSEN D.R., *Comparison of T1ρ, dGEMRIC, and quantitative T2 MRI in preoperative ACL rupture patients,* Acad Radiol, 2013, 20(1), 99-107.
33. LANKHORST N.E., BIERMA-ZEINSTRA S.M., VAN MIDDELKOOP M., *Factors associated with patellofemoral pain syndrome: a systematic review*, Br J Sports Med, 2013, 47(4), 193-206.
34. LEE D.W., YEOM C.H., KIM D.H., KIM T.M., KIM J.G., *Prevalence and Predictors of*

Patellofemoral Osteoarthritis after Anterior Cruciate Ligament Reconstruction with Hamstring Tendon Autograft, Clin Orthop Surg, 2018, 10(2), 181-190.

35. LEE S.M., YOON K.H., LEE S.H., HUR D., *The Relationship Between ACL Femoral Tunnel Position and Postoperative MRI Signal Intensity*, J Bone Joint Surg Am, 2017, 99(5), 379-387.
36. LI G., DEFRATE L.E., ZAYONTZ S., PARK S.E., GILL T.J., *The effect of tibiofemoral joint kinematics on patellofemoral contact pressures under simulated muscle loads*, J Orthop Res, 2004, 22(4), 801-806.
37. LIAO T.C., MARTINEZ A.G.M., PEDOIA V., MA B.C., LI X., LINK T.M., MAJUMDAR S., SOUZA R.B., *Patellar Malalignment Is Associated With Patellofemoral Lesions and Cartilage Relaxation Times After Hamstring Autograft Anterior Cruciate Ligament Reconstruction*, Am J Sports Med, 2020, 48(9), 2242-2251.
38. LUBOWITZ J.H., *Anatomic ACL reconstruction produces greater graft length change during knee range-of-motion than transtibial technique*, Knee Surg Sports Traumatol Arthrosc, 2014, 22(5), 1190-1195.
39. MARRA M.A., VANHEULE V., FLUIT R., KOOPMAN B.H., RASMUSSEN J., VERDONSCHOT N., ANDERSEN M.S., *A subject-specific musculoskeletal modeling framework to predict in vivo mechanics of total knee arthroplasty*, J Biomech Eng, 2015, 137(2), 020904.
40. NORTE G.E., KNAUS K.R., KUENZE C., HANDSFIELD G.G., MEYER C.H., BLEMKER S.S., HART J.M., *MRI-Based Assessment of Lower-Extremity Muscle Volumes in Patients Before and After ACL Reconstruction*, J Sport Rehabil, 2018, 27(3), 201-212.
41. PATTERSON B., CULVENOR A.G., BARTON C.J., GUERMAZI A., STEFANIK J., MORRIS H.G., WHITEHEAD T.S., CROSSLEY K.M., *Poor functional performance 1 year after ACL reconstruction increases the risk of early osteoarthritis progression*, Br J Sports Med, 2020, 54(9), 546-553.
42. PATTYN E., VERDONK P., STEYAERT A., VANDEN BOSSCHE L., VAN DEN BROECKE W., THIJS Y., WITVROUW E., *Vastus medialis obliquus atrophy: does it exist in patellofemoral pain syndrome?* Am J Sports Med, 2011, 39(7), 1450-1455.
43. PEARLE A.D., SHANNON F.J., GRANCHI C., WICKIEWICZ T.L., WARREN R.F.,

Comparison of 3-dimensional obliquity and anisometric characteristics of anterior cruciate ligament graft positions using surgical navigation, Am J Sports Med, 2008, 36(8), 1534-1541.

44. SAWILOWSKY S., *New Effect Size Rules of Thumb*, Journal of Modern Applied Statistical Methods, 2009, 8, 597-599.
45. SCHACHE A.G., SRITHARAN P., CULVENOR A.G., PATTERSON B.E., PERRATON L.G., BRYANT A.L., GUERMAZI A., MORRIS H.G., WHITEHEAD T.S., CROSSLEY K.M., *Patellofemoral joint loading and early osteoarthritis after ACL reconstruction*, J Orthop Res, 2023, 41(7), 1419-1429.
46. SHROUT P.E., FLEISS J.L., *Intraclass correlations: uses in assessing rater reliability*, Psychol Bull, 1979, 86(2), 420-428.
47. SKIPPER ANDERSEN M., DE ZEE M., DAMSGAARD M., NOLTE D., RASMUSSEN J., *Introduction to Force-Dependent Kinematics: Theory and Application to Mandible Modeling*, J Biomech Eng, 2017, 139(9), 091001.
48. SRITHARAN P., SCHACHE A.G., CULVENOR A.G., PERRATON L.G., BRYANT A.L., MORRIS H.G., WHITEHEAD T.S., CROSSLEY K.M., *Patellofemoral and tibiofemoral joint loading during a single-leg forward hop following ACL reconstruction*, J Orthop Res, 2022, 40(1), 159-169.
49. SRITHARAN P., SCHACHE A.G., CULVENOR A.G., PERRATON L.G., BRYANT A.L., CROSSLEY K.M., *Between-Limb Differences in Patellofemoral Joint Forces During Running at 12 to 24 Months After Unilateral Anterior Cruciate Ligament Reconstruction*, Am J Sports Med, 2020, 48(7), 1711-1719.
50. TAJIMA G., IRIUCHISHIMA T., INGHAM S.J., SHEN W., VAN HOUTEN A.H., AERTS M.M., SHIMAMURA T., SMOLINSKI P., FU F.H., *Anatomic double-bundle anterior cruciate ligament reconstruction restores patellofemoral contact areas and pressures more closely than nonanatomic single-bundle reconstruction*, Arthroscopy, 2010, 26(10), 1302-1310.
51. TAMPERE T., DEVRIENDT W., CROMHEECKE M., LUYCKX T., VERSTRAETE M., VICTOR J., *Tunnel placement in ACL reconstruction surgery: smaller inter-tunnel angles and higher peak forces at the femoral tunnel using anteromedial portal femoral drilling-a*

3D and finite element analysis, Knee Surg Sports Traumatol Arthrosc, 2019, 27(8), 2568-2576.

52. TRINLER U., SCHWAMEDER H., BAKER R., ALEXANDER N., *Muscle force estimation in clinical gait analysis using AnyBody and OpenSim*, J Biomech, 2019, 86, 55-63.
53. TSUKADA H., ISHIBASHI Y., TSUDA E., FUKUDA A., TOH S., *Anatomical analysis of the anterior cruciate ligament femoral and tibial footprints*, J Orthop Sci, 2008, 13(2), 122-129.
54. VICTOR J., LABEY L., WONG P., INNOCENTI B., BELLEMANS J., *The influence of muscle load on tibiofemoral knee kinematics*, J Orthop Res, 2010, 28(4), 419-428.
55. VIGNOS M.F., SMITH C.R., ROTH J.D., KAISER J.M., BAER G.S., KIJOWSKI R., THELEN D.G., *Anterior Cruciate Ligament Graft Tunnel Placement and Graft Angle Are Primary Determinants of Internal Knee Mechanics After Reconstructive Surgery*, Am J Sports Med, 2020, 48(14), 3503-3514.
56. WILLIAMS J.R., NEAL K., ALFAYYADH A., CAPIN J.J., KHANDHA A., MANAL K., SNYDER-MACKLER L., BUCHANAN T.S., *Patellofemoral contact forces and knee gait mechanics 3 months after ACL reconstruction are associated with cartilage degradation 24 months after surgery*, Osteoarthritis Cartilage, 2023, 31(1), 96-105.
57. WILLIAMS J.R., NEAL K., ALFAYYADH A., KHANDHA A., MANAL K., SNYDER-MACKLER L., BUCHANAN T.S., *Patellofemoral contact forces after ACL reconstruction: A longitudinal study*, J Biomech, 2022, 134, 110993.
58. WOO S.L., HOLLIS J.M., ADAMS D.J., LYON R.M., TAKAI S., *Tensile properties of the human femur-anterior cruciate ligament-tibia complex. The effects of specimen age and orientation*, Am J Sports Med, 1991, 19(3), 217-225.
59. ZHANG J., MA Y., PANG C., WANG H., JIANG Y., AO Y., *No differences in clinical outcomes and graft healing between anteromedial and central femoral tunnel placement after single bundle ACL reconstruction*, Knee Surg Sports Traumatol Arthrosc, 2021, 29(6), 1734-1741.